



Numerical Elastic Analysis of Functionally Graded (FG) Polar Orthotropic and Exponentially Varying-Thickness Rotating Disks via Combined Complementary Functions and the Transfer Matrix Methods

Vebil Yıldırım

Dept. of Mechanical Engineering, University of Çukurova, 01330 Adana, Turkey
E-mail address: vebil@cu.edu.tr

ORCID number of the author:
0000-0001-9955-8423

Received date: 10.02.2022
Accepted date: 31.05.2022

Abstract

In the present paper, the transfer matrix method (TMM) is to be employed for the first time in the open literature for the elastic analysis of variable-thickness disks made of functionally graded (FG) two orthotropic materials. Those materials are assumed to be continuously radially functionally graded (FG) based on the Voigt rule of mixture with two models. An exponential disk profile with two parameters is considered. Effects of the different boundary conditions (free-free, fixed-free, and fixed-fixed) and inhomogeneity indexes on the elastic response of the disk rotating at a constant angular speed are also examined. Additionally, direct numerical solutions of the problem with the complementary functions method (CFM) are presented in tabular forms together with the transfer matrix method solutions in which CFM was used as an assistant tool. It was observed that both location and amplitude of the maximum equivalent stress are affected by the grading models chosen. Such differences become more obvious for small values of the inhomogeneity indexes. The maximum relative error may reach 18% for the two material grading models in fixed-free disks. Consequently, Model-I may be recommended for just the inhomogeneity indexes equal to or greater than 0.5.

Keywords: Rotating disk, functionally graded, polar orthotropic, variable thickness, transfer matrix method, complementary functions method, initial value problem.

1. Introduction

Rotating disks are essential elements of turbine rotors, compressors, flywheels, automobile disc brake systems, gears, etc. Today's scientific works focus on the use of advanced materials so that discs can withstand much higher rotational speeds and resulting stresses.

To serve the purpose above mentioned, ordinary anisotropic materials have been examined [1-24]. The mechanical benefits of a material gradient may be significant in the design of such structures to enhance structural performance. As a class of nonhomogeneous isotropic advanced materials, low-cost functionally graded (FG) metal-ceramics play a significant role in this subject area [25-51]. Based on a chosen material grading rule, material properties may vary continuously along with one or more certain directions in FG metal-ceramics. From those, Eraslan and Akış [28] worked on the elastic analysis of FG parabolically-varying thickness disks. Based on a semi-analytical axisymmetric elastic solution, Bayat et al. [31] considered rotating hollow parabolic and hyperbolic disks. Hojjati and Jafari [34] introduced two analytical methods, namely the homotopy perturbation method (HPM) and Adomian's decomposition method (ADM), to obtain stresses and displacements in rotating disks with



variable thicknesses and densities. They also compared the result with the verified variational iteration method (VIM) solution. The comparison among the methods used in Ref. [34] showed that although the numerical results were almost the same, HPM is much easier, more convenient, and more efficient than ADM and VIM. Hojjati and Hassani [35] conducted a stress-strain analysis of rotating discs with nonuniform thickness and density for an elastic-linear hardening disk material. They used variable material properties (VMP) theory for a theoretical solution, Runge-Kutta's method for a numerical solution, and commercial finite element modeling for comparisons of their results. They suggested the VMP method which provides reliable means for complex discs. Nie and Batra [36] analyzed axisymmetric deformations of a rotating FGM nonuniform disk made of a rubberlike material that was modeled as isotropic, linear thermoelastic, and incompressible by using an Airy stress function and the differential quadrature method. They [36] also worked on the material tailoring for obtaining a constant linear combination of the hoop stress and the radial stress. By dividing the variable-thickness disk into sub-domains with uniform thickness, Hassani et al. [38] studied the elastic behavior of rotating FG- isotropic hyperbolic rotating disks based on of a semi-exact method of Liao's homotopy analysis. Nejad et al. [41-42] examined exponentially FG disks subjected to internal and external pressures [41] and centrifugal forces [42]. Yildirim [44] analytically formulated the exact elastic response of a power-law graded hyperbolic rotating disk subjected to the internal and external pressures including a rotation at a constant angular velocity under four physical boundary conditions. Based on both complementary functions and transfer matrix methods, Yildirim and Kacar [45] introduced a versatile computer package program for the elastic analysis of arbitrarily FG-isotropic thick-walled annular structures under all possible boundary conditions, namely variable thickness disks, cylinders, and spheres. Gang [47] analytically studied the stress analysis of a simple-power law graded hyperbolic free-free rotating disk for four convergent disk profiles and negative inhomogeneity indexes. Yildirim [48] presented a comprehensive parametric study for a power-law graded hyperbolic rotating disk. Based on the transfer matrix approach, Yildirim [49], considered six different material grading rules such as a simple power rule (P-FGM), an exponential function (E-FGM), a linear function (L-FGM), a Voigt mixture rule with the power of volume fractions of constituents (V-FGM), a Mori-Tanaka scheme (MT-FGM), and a sigmoid function (S-FGM) with several parabolically/linearly/hyperbolically tapered disk profiles including uniform ones to study the elastic response of rotating disks made of FG metal and ceramic pairs (Al/Al_2O_3) under free-free, fixed-free, and fixed-fixed boundary conditions. The computer program introduced in [45] was used in Yildirim's [49] study, and the transfer matrix was obtained with the help of the complementary functions method as in the present study. Khorsand and Tang [50], recently, employed an advanced algorithm to optimize the weight of a hollow FG varied thickness disk under thermoelastic loads based on a combination of a co-evolutionary particle swarm optimization (CPSO) approach coupled with a differential quadrature (DQ).

In quest of searching for more advanced materials, the mechanical benefits of a material gradient have begun to be probed into anisotropic materials [51-61] instead of isotropic ones [25-50]. This group of materials, which are mainly in the scope of the present study, are called functionally graded (FG) anisotropic materials or are referred to as anisotropic and inhomogeneous materials. There are, unfortunately, a very limited number of works on FG disks composed of anisotropic materials in the open literature [51-61]. Among these, Durodola and Attia [51] studied elastic stresses in a rotating hollow uniform disk made from FG orthotropic materials. Chen et al. [52] presented a 3-D analytical solution for a uniform transversely isotropy exponentially FG rotating disk. Nie et al. [53] calculated numerically the required radial variation of the volume fraction of fibers for a rotating annular CR-disk composed of a fiber-reinforced composite. Kansal and Parvez [54] carried out stress analysis of orthotropic graded rotating annular disks under a parabolic temperature distribution. Lubarda [55] worked on the elastic response of uniformly pressurized cylindrically anisotropic hollow

uniform thin rotating disks by using both the finite difference method and a Fredholm integral equation. Peng and Li [56] also employed a Fredholm integral equation for elastic analysis of a hollow FG polar-orthotropic rotating disk under free-free and fixed-free boundary conditions. After deriving a confluent hypergeometric differential equation, Essa and Argeso [58] studied analytically and numerically the effects of the anisotropy degree on the elastic fields of polar orthotropic FG annular free-free and fixed-free rotating variable-thickness disks. Based on the finite difference method and Voigt mixture grading rule with powers, Zheng et al. [59] numerically studied elastic fields in a fiber-matrix FG variable thickness circumferentially aligned (CR) disk mounted on a rotating shaft and subjected to an angular deceleration. Zheng et al.'s [59] study revealed that disk deceleration has no effect on the radial and hoop stresses except the shear stress. As an extension of Ref. [57], Yıldırım [60] proposed closed-form solutions for the elastic fields in a simple power-law graded polar orthotropic hyperbolically tapered disk under separate inner/outer pressures, and centrifugal forces due to the rotation at a constant angular speed. Yıldırım's [60] formulas are capable of exact determination of the elastic behavior of continuously hyperbolically tapered disks made of a single isotropic material, made of a single polar orthotropic material, or made of a nonhomogeneous material formed by functionally power-law graded two isotropic materials, or a nonhomogeneous material formed by functionally power-law graded two orthotropic materials. As the latest study in the related realm, Yıldırım [61] numerically investigated the elastic response of arbitrarily functionally graded polar orthotropic rotating disks having constant thickness. Anisotropy effects on the elastic response were examined numerically with both simple power and exponential material grading rules with the help of only complementary functions method (CFM). CFM solutions were verified with closed-form solutions to simple power gradation rule and uniform disks.

As seen from the open literature that there are just three studies conducted by Essa and Argeso [58], Zheng et al. [59], and Yıldırım [60] on the elastic response of variable-thickness FG polar orthotropic rotating disks. The last work [60] is an analytical study which considers just hyperbolic thickness variation, and the simple-power material grading pattern. This was a great motivation for the author.

This study is a continuation of References [45, 49, 60-61] to study the elastic response of exponentially varying thickness FG polar orthotropic rotating disks based on the combined complementary functions and the transfer matrix methods. As stated above, Yıldırım [49] used the transfer matrix method previously as in the present study for the variable thickness disks (parabolic, hyperbolic, and linearly varying) made of FG two isotropic materials that are metallic and ceramic ($E_r(r) = E_\theta(r) = E(r)$ and $\nu_{r\theta} = \nu_{\theta r} = \nu$). Yıldırım [49] revealed that the free-free and fixed-free variable thickness disks show better performance than the uniform ones under centrifugal forces. The present study also aims to compare the results of the frequently used two Voigt models for the gradation of two orthotropic materials. The author hopes that the findings of the present study will be very helpful to engineers and academicians.

2. Mathematical Formulation and Solution of the Problem

Under small deformations and a state of axisymmetric plane stress assumptions for thin plates, field equations of a variable thickness rotating nonhomogeneous disk made of a linear elastic polar orthotropic material in polar coordinates (r, θ) are reduced to [60]

$$\varepsilon_r(r) = \frac{du_r(r)}{r}, \quad \varepsilon_\theta(r) = \frac{u_r(r)}{r} \quad (1a)$$

$$\begin{aligned} \sigma_r(r) &= -\frac{E_\theta(r)v_{r\theta}}{v_{\theta r}(v_{r\theta}v_{\theta r} - 1)}\varepsilon_r(r) - \frac{E_\theta(r)v_{r\theta}}{(v_{r\theta}v_{\theta r} - 1)}\varepsilon_\theta(r) \\ &= C_{11}(r)\varepsilon_r(r) + C_{12}(r)\varepsilon_\theta(r) \end{aligned} \quad (1b)$$

$$\sigma_\theta(r) = -\frac{E_\theta(r)v_{r\theta}}{(v_{r\theta}v_{\theta r} - 1)}\varepsilon_r(r) - \frac{E_\theta(r)}{(v_{r\theta}v_{\theta r} - 1)}\varepsilon_\theta = C_{12}(r)\varepsilon_r(r) + C_{22}(r)\varepsilon_\theta(r) \quad (1c)$$

$$(h(r)r\sigma_r(r))' - h(r)\sigma_\theta(r) + \rho(r)h(r)\omega^2r = 0 \quad (1d)$$

where Eq. (1a) is called the strain-displacement relations, Eqs. (1b) and (1c) are referred to as linear elastic stress-strain relations, and finally, Eq. (1d) is the equilibrium equation under the centrifugal forces. In Eq. (1), $u_r(r)$ is the radial displacement, $\varepsilon_r(r)$ and $\varepsilon_\theta(r)$ are the radial and circumferential strains, respectively; $\sigma_r(r)$ is the radial stress, $\sigma_\theta(r)$ is the hoop stress, ω is the constant angular velocity, $\rho(r)$ is the material density, $h(r)$ is the disk thickness profile, $E_r(r)$ and $E_\theta(r)$ are Young's moduli along the radial and tangential directions, respectively; $C_{ij}(r)$ are the transformed on-axis in-plane stiffness terms ($E_1 = E_r, E_2 = E_\theta, \nu_{12} = \nu_{r\theta}$), in addition $\nu_{r\theta}$ and $\nu_{\theta r}$ are anisotropic Poisson's ratios assumed to be constant in the formulation. Those anisotropic Poisson's ratios are also related by Maxwell's theorem as follows

$$\frac{\nu_{\theta r}}{E_\theta(r)} = \frac{\nu_{r\theta}}{E_r(r)} \quad (2)$$

It is worth noting that, the radial and circumferential strains must obey the following compatibility equation

$$\frac{d}{dr}(r\varepsilon_\theta(r)) - \varepsilon_r(r) = 0 \quad (3)$$

Navier equation which is in the form of a second-order differential equation with variable coefficients is derived from the field equations given in Eq. (1) as follows

$$\frac{d^2u_r(r)}{dr^2} + \left(\frac{1}{r} + \frac{\frac{dC_{11}(r)}{dr}}{C_{11}(r)} \right) \frac{du_r(r)}{dr} + \left(\begin{array}{c} -\frac{C_{22}(r)}{r^2C_{11}(r)} \\ +\frac{C_{12}(r)}{rC_{11}(r)} \left(\frac{\frac{dC_{11}(r)}{dr}}{C_{11}(r)} + \frac{\frac{dh(r)}{dr}}{h(r)} \right) \end{array} \right) u_r(r) = -\frac{\rho(r)\omega^2r}{C_{11}(r)} \quad (4)$$

Equation (4) may be solved by using a technique developed for the solution of two-point boundary value problems (BVP), or it may be handled by a technique like transfer matrix [1,49,62-69] and complementary functions methods [24,61,70-75] or any of the others developed for the solution of initial value problems (IVP).

The principal aim of the present study is to make use of the transfer matrix method in the solution of such kinds of problems. The transfer matrix method allows accurate and economical

solutions to more complicated problems which may be presented in future works. As a by-product, direct solutions to the same problem considered by the complementary functions method are also to be tabulated in the present work.

To employ the transfer matrix method, firstly, Eq. (4) should be written as a first-order differential equation set as follows

$$\frac{du_r(r)}{dr} = -\frac{E_\theta(r)v_{r\theta}}{rE_r(r)}u_r(r) - \frac{(v_{r\theta}v_{\theta r} - 1)}{E_r(r)}\sigma_r(r) \quad (5a)$$

$$\frac{d\sigma_r(r)}{dr} = -\frac{E_\theta(r)(E_r(r) - E_\theta(r)v_{r\theta}^2)}{r^2E_r(r)(v_{r\theta}v_{\theta r} - 1)}u_r(r) + \left(\frac{E_\theta(r)v_{r\theta}}{rE_r(r)} - \frac{1}{r} - \frac{dh(r)}{h(r)dr} \right)\sigma_r(r) - \rho(r)\omega^2r \quad (5b)$$

Equation (5) is written in a more compact form of

$$\frac{d\mathbf{S}(r)}{dr} = \mathbf{D}(r)\mathbf{S}(r) + \mathbf{f}(r) \quad (6)$$

where $\mathbf{D}(r)$ is the differential matrix, $\mathbf{S}(r)$ is the state vector and $\mathbf{f}(r)$ is the nonhomogeneous vector.

$$\mathbf{S}(r) = \begin{Bmatrix} u_r(r) \\ \sigma_r(r) \end{Bmatrix} \quad (7a)$$

$$\mathbf{f}(r) = \begin{Bmatrix} 0 \\ -\rho(r)\omega^2r \end{Bmatrix} \quad (7b)$$

In the transfer matrix method, the general solution of Eq. (6) is given by [62]

$$\mathbf{S}(r) = \mathbf{F}(a, r)\mathbf{S}(a) + \int_a^r \mathbf{F}(\xi, r)\mathbf{f}(\xi)d\xi \quad (8)$$

In a few words, If both $\mathbf{F}(a, r)$ and $\mathbf{S}(a)$ are known in Eq. (8), then both the radial displacement and the radial stress are obtained at any surface of the disk in a straight forward. For the circumferential stress, utilizing Eq. (1), the following may also be written

$$\sigma_\theta(r) = \left(\frac{C_{11}^2(r) - C_{12}^2(r)}{C_{11}(r)} \right) \frac{u_r(r)}{r} + \left(\frac{C_{12}(r)}{C_{11}(r)} \right) \sigma_r(r) \quad (9)$$

On the eve of the application of Eq. (8), both the overall transfer matrix and, then, the unknown elements of the initial state vector, $\mathbf{S}(a)$, should be determined. If the elements of the differential matrix are not a function of the radial coordinate, then, it is possible to obtain a closed-form solution for the transfer matrix elements [49, 62, 69]. Otherwise, a numerical solution technique like the complementary functions method as in the present study or any ordinary differential equation set solver in the case of variable coefficients may be used. As

may be guessed from Eq. (5), since the elements of the differential matrix become more complex functions due to the variation of both the material and geometrical properties of the disk, it is suitable to solve directly the related differential equations instead of using some approximate methods to get much more accurate elements of the transfer matrix. Both the material orthotropy [61] and the thickness gradient [49] significantly influence the accuracy of the transfer matrix.

The transfer matrix satisfies a similar differential equation with the state vector in Eq. (6) in case of $f(r) = 0$.

$$\frac{d\mathbf{F}(a, r)}{dr} = \mathbf{D}(r)\mathbf{F}(a, r) \quad (10)$$

The numerical solution of Eq. (10) under Kronecker delta initial boundary conditions gives the transfer matrix in the numerical form [62-63,73-75]

$$\mathbf{F}(a, a) = \mathbf{I} \quad (11)$$

In Eq. (11), \mathbf{I} is the unit matrix. In the present study, the numerical solution of Eq. (10) under boundary conditions given in Eq. (11) was achieved with the help of the complementary functions method whose details were presented in References [24, 61]. This combined technique has already been used successfully in some of the author's previous studies [73-75].

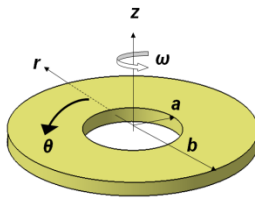
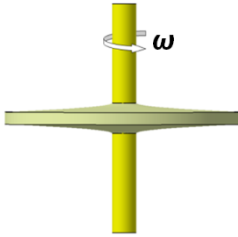
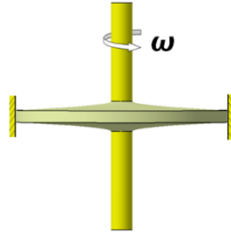
Immediately after the numerical determination of the transfer matrix, the unknown elements of the initial state vector may be established. To do this, Eq. (8) is written at $r = b$, the boundary conditions given at inner and outer surfaces are then implemented into the equation. The boundary conditions considered in the present study are presented in Table 1. After implementation of those boundary conditions, the whole elements of the initial state vector are calculated from the following equations (see Appendix).

$$\mathbf{S}(a)_{Free-Free} = \begin{Bmatrix} u_r(a) \\ \sigma_r(a) \end{Bmatrix} = \begin{Bmatrix} \omega^2 \int_a^b F_{2,2}(\xi, r) \rho(\xi) \xi d\xi \\ F_{2,1}(a, b) \\ 0 \end{Bmatrix} \quad (12a)$$

$$\mathbf{S}(a)_{Fixed-Free} = \begin{Bmatrix} u_r(a) \\ \sigma_r(a) \end{Bmatrix} = \begin{Bmatrix} 0 \\ \omega^2 \int_a^b F_{2,2}(\xi, r) \rho(\xi) \xi d\xi \\ F_{2,2}(a, b) \end{Bmatrix} \quad (12b)$$

$$\mathbf{S}(a)_{Fixed-Fixed} = \begin{Bmatrix} u_r(a) \\ \sigma_r(a) \end{Bmatrix} = \begin{Bmatrix} 0 \\ \omega^2 \int_a^b F_{1,2}(\xi, r) \rho(\xi) \xi d\xi \\ F_{1,2}(a, b) \end{Bmatrix} \quad (12c)$$

Table 1. Boundary conditions considered [44]

Free-Free	Fixed-Free	Fixed-Fixed
		
$\sigma_r(a) = 0$ $\sigma_r(b) = 0$	$u_r(a) = 0$ $\sigma_r(b) = 0$	$u_r(a) = 0$ $u_r(b) = 0$

3. Verifications of the Results

For the sake of simplicity, the application of this method may be shown on the simple model of Eq. (5) governs the elasto-static behavior of non-uniform disks made of any arbitrarily continuously graded polar orthotropic materials. The disk thickness may vary along the radial coordinate according to any differentiable function.

In the present study, a two-parameter exponential function proposed by Eraslan and Orcan [76] is studied with $a = 0.01m, b = 0.1m, h_o = a, m = 0.6,$ and $k = 0.8$ (Fig. 1).

$$h(r) = h_o e^{-m(\frac{r}{b})^k} \tag{13}$$

In the present study, a simple Voigt mixture rule is utilized with a power of volume fraction of constituents based on the two models (Fig. 2)

$$V_B^I = \left(\frac{r-a}{b-a}\right)^n, n \geq 0 \tag{14a}$$

$$V_B^{II} = \left(\frac{r^n - a^n}{b^n - a^n}\right), n > 0 \tag{14b}$$

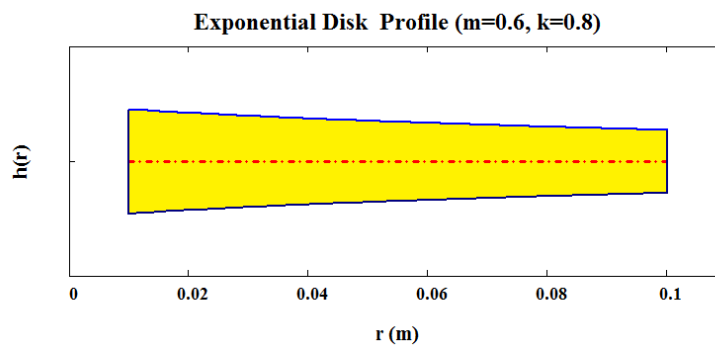


Fig. 1. The exponential disk profile

Where n is called the inhomogeneity parameter, V_B stands for the volume fraction of *Material – B*, superscripts show the model number. The radial variation of the effective material properties such as $E_r(r)$, $E_\theta(r)$, and $\rho(r)$ are then defined by the following expression.

$$P(r) = P_A V_A + P_B V_B = P_A(1 - V_B) + P_B V_B = (P_B - P_A)V_B + P_A \quad (15)$$

In Eq. (15), the outer surface is to be *Material – B* rich (woven Glass fiber/Epoxy prepreg) while the inner surface is *Material – A* rich (An injection molded Nylon 6 composite containing 40 wt% short glass fiber) (Table 2). The same gradation of Eq. (14b) was originally used by Peng and Li [56] for uniform thickness polar orthotropic FG annular disks.

It is worth noting that, in the present numerical analysis, the arithmetic mean of anisotropic Poisson’s ratios of two orthotropic materials is considered.

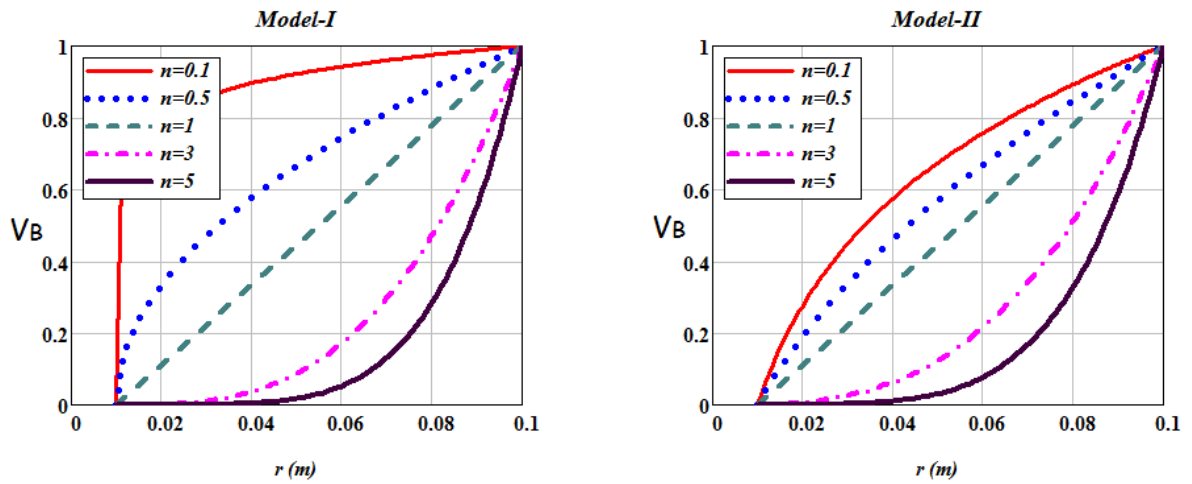


Fig. 2. Volume fraction models considered in this work

Table 2. Anisotropic constituent materials and their properties.

	E_r (GPa)	E_θ (GPa)	ρ (kg/m ³)	$\nu_{r\theta}$
<i>Material – A</i> [19-20, 56]	12.0	20.0	1600	0.21
<i>Material – B</i> [19-20]	21.8	26.95	2030	0.15

4. Validation of the Present Formulation

The followings are used for dimensionless displacement and stresses

$$\bar{u}_r = \frac{E_o}{\rho_o \omega^2 b^3} u_r, \bar{\sigma}_r = \frac{\sigma_r}{\rho_o \omega^2 b^2}, \bar{\sigma}_\theta = \frac{\sigma_\theta}{\rho_o \omega^2 b^2} \quad (16)$$

In this section, $\sigma_o = 12 \text{ GPa}$, $\rho_o = 1600 \text{ kg/m}^3$ have been used in Eq. (16) to calculate the non-dimensional elastic fields in a uniform rotating disk made of FG orthotropic materials having properties given in Table 2. Peng and Li [56] studied this disk of $a/b = 0.4$ by using Model-II in Eq. (14b). The main difference between the present study and Ref. [56] is that the constant value of anisotropic Poisson's ratios is taken differently. That is, Peng and Li [56] used $\nu_{r\theta} = 0.21 = \text{constant}$ along the radial coordinate while the present study considers the arithmetic mean of Poisson's ratios, $\nu_{r\theta} = 0.18 = \text{constant}$. Since Ref. [56] presented the results in graphical forms, the comparison is to be made in Fig. 3. A perfect harmony can be seen in Fig. 3. Very minor differences in the values of the radial displacement may be due to the value of Poisson's ratio used.

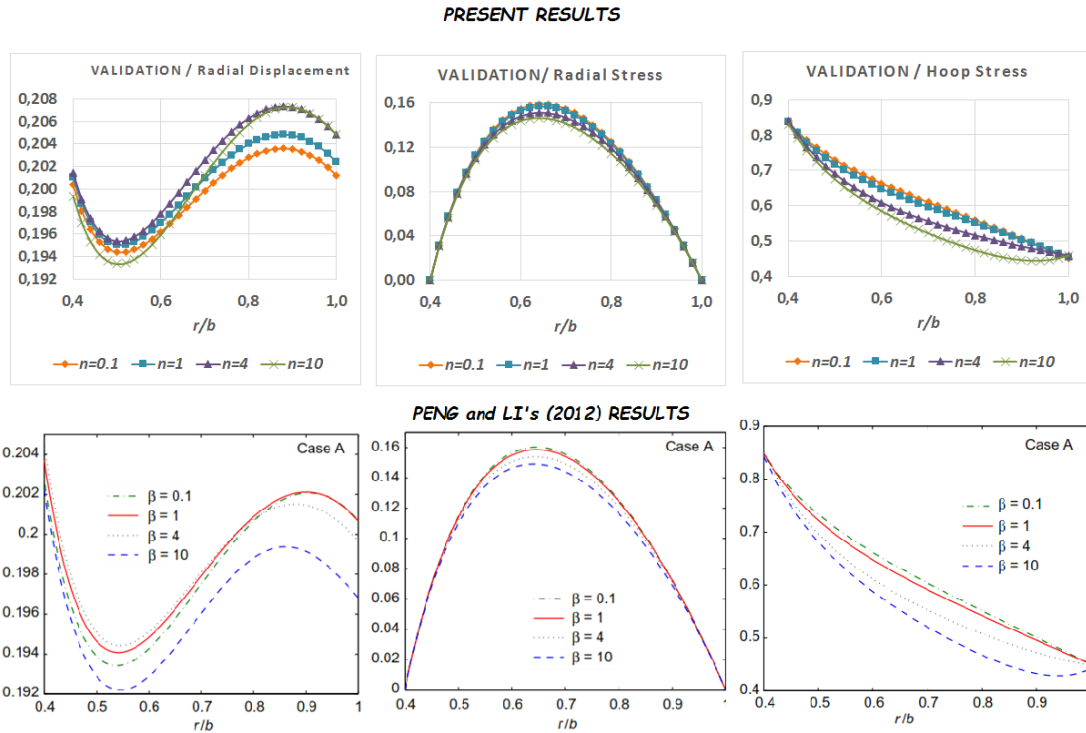


Fig. 3. Validation of the present dimensionless results with the open literature ($\sigma_o = 12 \text{ GPa}$, $\rho_o = \frac{1600 \text{ kg}}{\text{m}^3}$, Free – Free)

5. Numerical Examples

Unless otherwise stated, $\sigma_o = 20 \text{ GPa}$, $\rho_o = 1600 \text{ kg/m}^3$ are to be used in the calculation of dimensionless quantities in Eq. (16) for a non-uniform disk of $a/b = 0.1$ in this section. Dimensionless elastic fields under free-free, fixed-free, and fixed-fixed boundary conditions are illustrated in Figs. 4-6 based on the two models.

For the aim of comparison of the transfer matrix method (TMM) and the complementary functions method (CFM) solutions for an exponential disk based on the two models with $n=3$, some numerical results are given in the tabular form in Tables 3 and 4. In those tables, the equivalent von-Mises stress under plane stress assumption is defined by

$$\sigma_{eq} = \sqrt{\sigma_r^2 - \sigma_r\sigma_\theta + \sigma_\theta^2} \quad (17)$$

When comparing two models (Fig. 2), minor differences are observed in the variation of the same elastic properties for inhomogeneity indexes greater than the unit. However, when the inhomogeneity index approaches zero, viz., when the inhomogeneity index is strictly less than the unit, the significant differences become obvious. The effects of these on the numerical values of the elastic fields are to be discussed below.

From Figs. 4-6, it is mostly observed that as n increases the maximum displacement also increases while both the maximum radial stress and circumferential stress decrease. Those figures also show that the maximum radial dimensionless displacement is located at the outer surface under both free-free and fixed-free boundary conditions. However, it is in the vicinity of the mid surface, at $r/b \cong 0.6$, for fixed-fixed boundaries. Model-II gives slightly higher maximum radial displacements than Model-I:

$$\begin{aligned} \bar{u}_r^I{}_{max} &= 0.195274, & \bar{u}_r^{II}{}_{max} &= 0.2048695 \rightarrow \text{at } r = b \text{ with } n = 0.1 \text{ (FREE - FREE)} \\ \bar{u}_r^I{}_{max} &= 0.1877075, & \bar{u}_r^{II}{}_{max} &= 0.1985936 \rightarrow \text{at } r = b \text{ with } n = 0.1 \text{ (FIXED - FREE)} \\ \bar{u}_r^I{}_{max} &= 0.05018 \rightarrow \text{at } r/b = 0.618 \text{ with } n = 0.1 \text{ (FIXED - FIXED)} \\ \bar{u}_r^{II}{}_{max} &= 0.05207 \rightarrow \text{at } r/b = 0.595 \text{ with } n = 0.1 \text{ (FIXED - FIXED)} \end{aligned}$$

As to the maximum radial stress (Figs. 4-6), it is approximately at $r/b \cong 0.4$ under free-free conditions, at the inner surface under fixed-free boundaries, and at the outer surface under fixed-fixed boundary conditions. The maximum radial stress is in compression at fixed-fixed surfaces:

$$\begin{aligned} \bar{\sigma}_r^I{}_{max} &= 0.32585 \rightarrow \text{at } r/b = 0.393 \text{ with } n = 0.1 \text{ (FREE - FREE)} \\ \bar{\sigma}_r^{II}{}_{max} &= 0.30113 \rightarrow \text{at } r/b = 0.415 \text{ with } n = 0.1 \text{ (FREE - FREE)} \\ \bar{\sigma}_r^I{}_{max} &= 0.4797, & \bar{\sigma}_r^{II}{}_{max} &= 0.383458 \rightarrow \text{at } r = a \text{ with } n = 0.1 \text{ (FIXED - FREE)} \\ \bar{\sigma}_r^I{}_{max} &= -0.3232780, & \bar{\sigma}_r^{II}{}_{max} &= -0.3229234 \rightarrow \text{at } r = b \text{ with } n = 0.1 \text{ (FIXED - FIXED)} \end{aligned}$$

From the above, a major difference between the two models is observed in the maximum radial stress at the inner surface for $n = 0.1$.

Let's now consider the maximum tangential stresses (Figs. 4-6). It is located immediately before or at just the inner surface under free-free boundary conditions, and at around mid-surface under both fixed-free (at $r/b \cong 0.5$) and fixed-fixed (at $r/b \cong 0.3$) conditions:

$$\begin{aligned} \bar{\sigma}_\theta^I{}_{max} &= 0.59 \rightarrow \text{at } r/b = 0.122 \text{ with } n = 0.1 \text{ (FREE - FREE)} \\ \bar{\sigma}_\theta^{II}{}_{max} &= 0.58 \rightarrow \text{at } r = a \text{ with } n = 0.1 \text{ (FREE - FREE)} \\ \bar{\sigma}_\theta^I{}_{max} &= 0.397 \rightarrow \text{at } r/b = 0.46 \text{ with } n = 0.1 \text{ (FIXED - FREE)} \\ \bar{\sigma}_\theta^{II}{}_{max} &= 0.400 \rightarrow \text{at } r/b = 0.483 \text{ with } n = 0.1 \text{ (FIXED - FREE)} \\ \bar{\sigma}_\theta^I{}_{max} &= 0.161, & \bar{\sigma}_\theta^{II}{}_{max} &= 0.155 \rightarrow \text{at } r/b = 0.325 \text{ with } n = 0.1 \text{ (FIXED - FIXED)} \end{aligned}$$

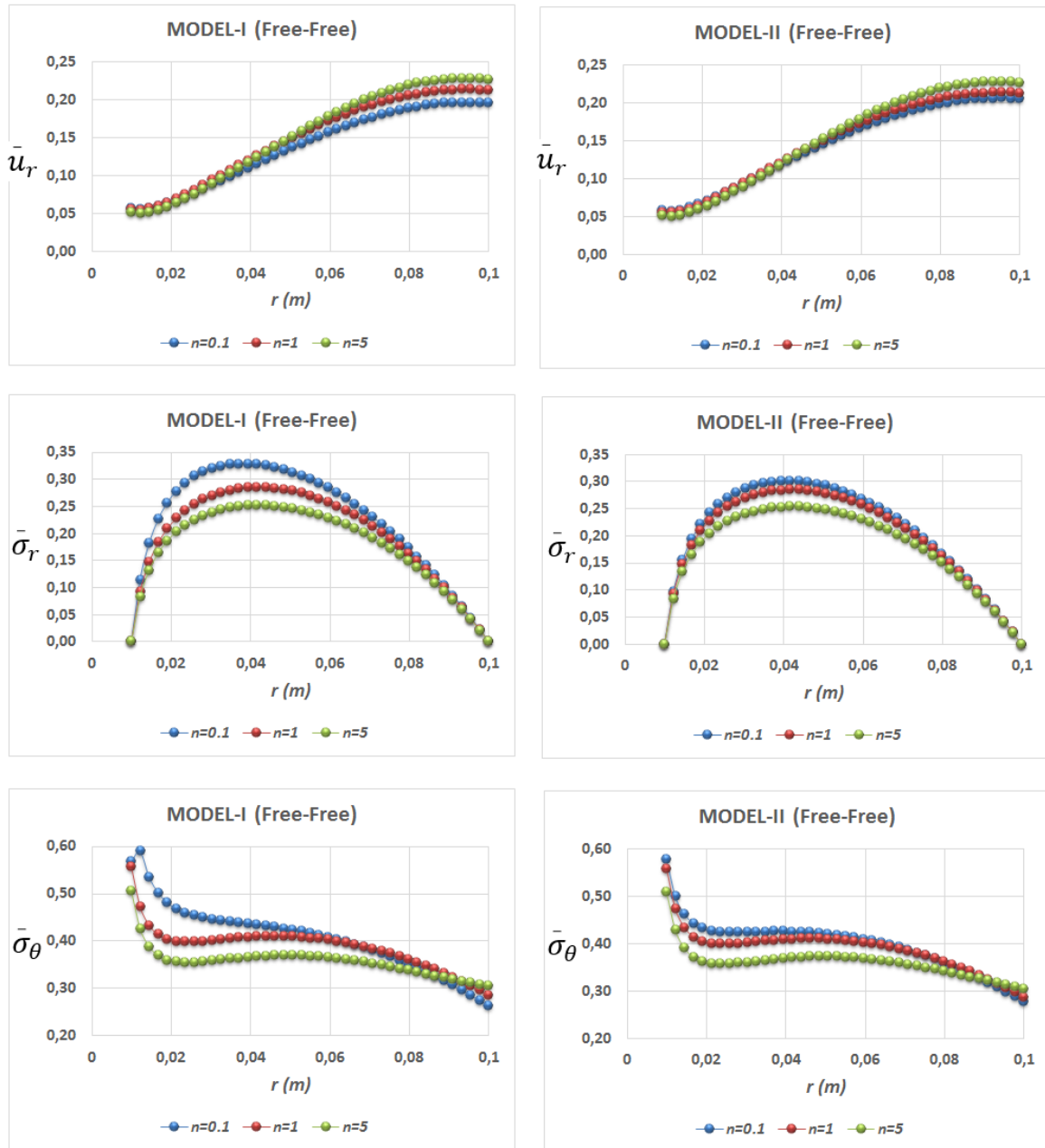


Fig. 4. Dimensionless elastic fields under free-free boundary conditions

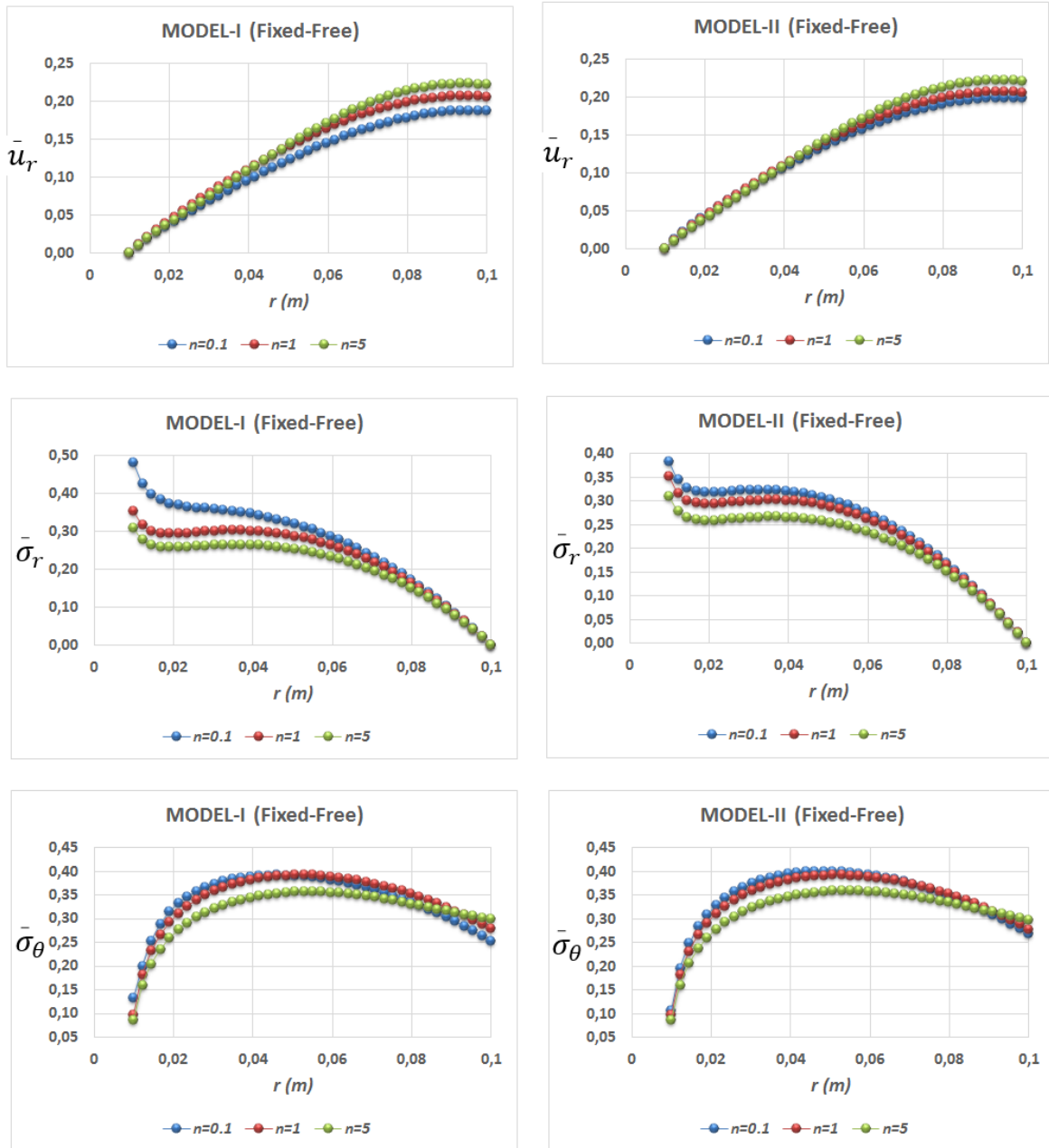


Fig. 5. Dimensionless elastic fields under fixed-free boundary conditions

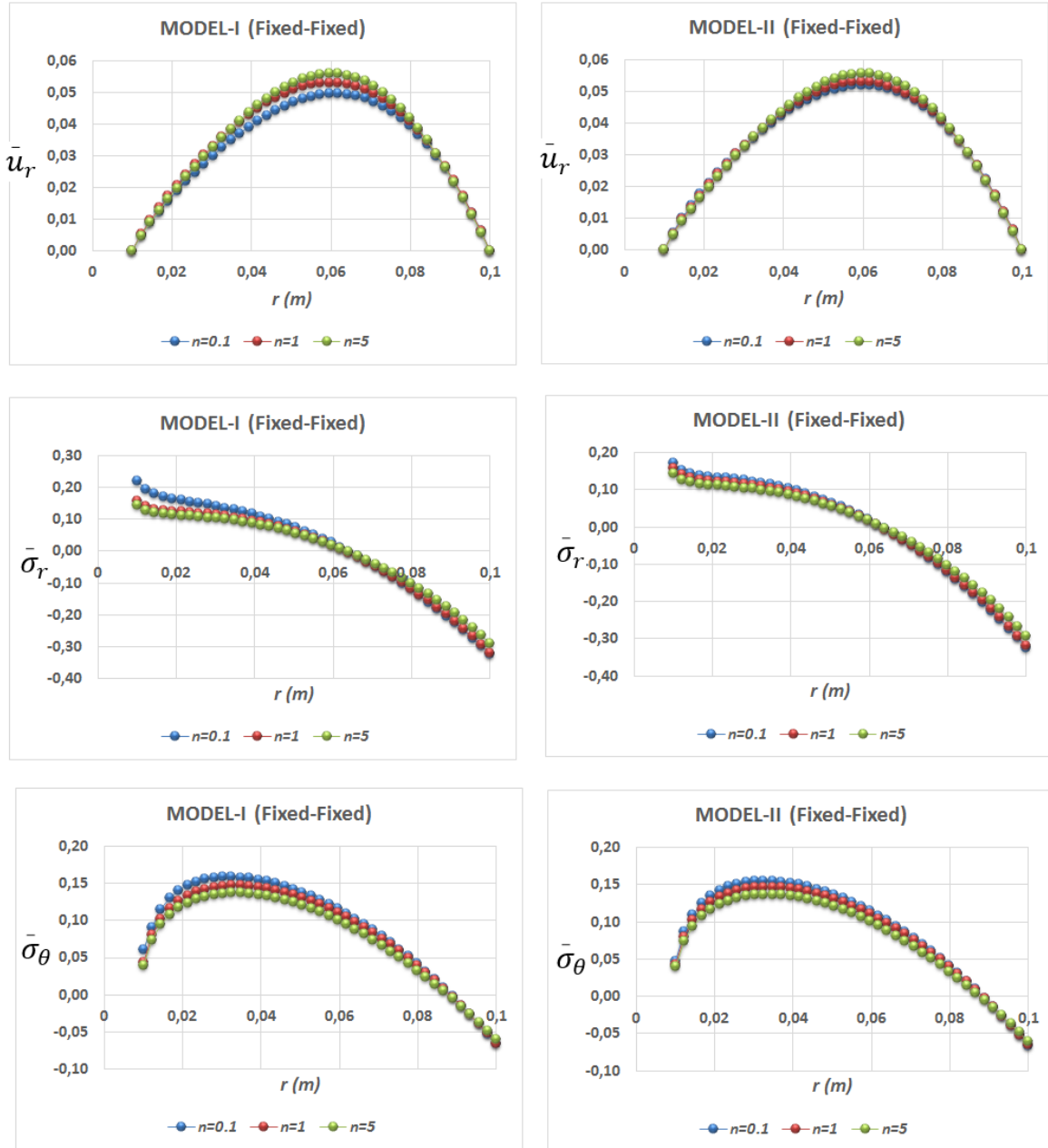


Fig. 6. Dimensionless elastic fields under fixed-fixed boundary conditions

The maximum equivalent stress is located at the inner surface under free-free boundary conditions while it is at the outer surface for fixed-fixed ones (Fig. 7). From Fig. 7, a clear difference between the two models is observed in the value and location of the maximum equivalent stress under fixed-free boundary conditions.

$$(\bar{\sigma}_{eq})_{max}^I = 0.4291, \quad (\bar{\sigma}_{eq})_{max}^{II} = 0.3430 \rightarrow \text{at } r = a \text{ with } n = 0.1 \text{ (FIXED - FREE)}$$

$$(\bar{\sigma}_{eq})_{max}^{II} = 0.3645, \quad (\bar{\sigma}_{eq})_{max}^I = 0.37 \rightarrow \text{at } r/b = 0.438 \text{ with } n = 0.1 \text{ (FIXED - FREE)}$$

Table 3. Comparisons of the transfer matrix method (TMM) and the complementary functions method (CFM) elastic fields in the exponential disk based on the Model-I (n=3)

$r(m)$	\bar{u}_r		$\bar{\sigma}_r$		$\bar{\sigma}_\theta$		$\bar{\sigma}_{eq}$	
	CFM	TMM	CFM	TMM	CFM	TMM	CFM	TMM
Free-Free								
0.01	0.05174	0.05174	0.00000	0.00000	0.51742	0.51742	0.51742	0.51742
0.019	0.05994	0.05994	0.19084	0.19082	0.36828	0.36823	0.31901	0.31897
0.028	0.08367	0.08366	0.23928	0.23925	0.36548	0.36543	0.32152	0.32148
0.037	0.11157	0.11156	0.25696	0.25692	0.37444	0.37440	0.33169	0.33165
0.046	0.13999	0.13997	0.25840	0.25836	0.38041	0.38036	0.33643	0.33638
0.055	0.16659	0.16657	0.24710	0.24706	0.38065	0.38060	0.33451	0.33446
0.064	0.18955	0.18953	0.22391	0.22387	0.37490	0.37485	0.32671	0.32667
0.073	0.20747	0.20744	0.18866	0.18862	0.36362	0.36357	0.31498	0.31493
0.082	0.21942	0.21939	0.14055	0.14051	0.34742	0.34738	0.30270	0.30267
0.091	0.22494	0.22493	0.07827	0.07825	0.32679	0.32676	0.29553	0.29551
0.1	0.22399	0.22399	0.00000	0.00000	0.30183	0.30183	0.30183	0.30183
Fixed-Free								
0.01	0.00000	0.00000	0.31646	0.31646	0.08738	0.08738	0.28308	0.28307
0.019	0.03653	0.03653	0.26398	0.26400	0.26518	0.26521	0.26459	0.26460
0.028	0.06899	0.06899	0.26941	0.26942	0.32118	0.32120	0.29867	0.29870
0.037	0.10094	0.10095	0.27276	0.27278	0.34975	0.34978	0.31831	0.31834
0.046	0.13161	0.13162	0.26778	0.26780	0.36430	0.36433	0.32691	0.32693
0.055	0.15958	0.15959	0.25304	0.25306	0.36889	0.36892	0.32675	0.32678
0.064	0.18340	0.18341	0.22776	0.22778	0.36554	0.36557	0.31975	0.31978
0.073	0.20187	0.20189	0.19110	0.19113	0.35563	0.35566	0.30827	0.30830
0.082	0.21418	0.21419	0.14198	0.14200	0.34022	0.34025	0.29598	0.29600
0.091	0.21992	0.21993	0.07892	0.07893	0.32001	0.32003	0.28876	0.28877
0.1	0.21910	0.21910	0.00000	0.00000	0.29523	0.29523	0.29523	0.29523
Fixed-Fixed								
0.01	0.00000	0.00000	0.14401	0.14401	0.03976	0.03976	0.12882	0.12882
0.019	0.01622	0.01622	0.11362	0.11363	0.11676	0.11677	0.11522	0.11523
0.028	0.02946	0.02946	0.10540	0.10541	0.13450	0.13451	0.12257	0.12258
0.037	0.04080	0.04080	0.09165	0.09166	0.13630	0.13631	0.12036	0.12037
0.046	0.04938	0.04939	0.06926	0.06927	0.12832	0.12833	0.11124	0.11125
0.055	0.05415	0.05415	0.03727	0.03728	0.11247	0.11248	0.09923	0.09924
0.064	0.05420	0.05420	-0.0051	-0.0051	0.08975	0.08976	0.09240	0.09241
0.073	0.04891	0.04892	-0.0588	-0.0588	0.06080	0.06081	0.10356	0.10356
0.082	0.03803	0.03804	-0.1250	-0.1250	0.02596	0.02597	0.13980	0.13980
0.091	0.02163	0.02163	-0.2054	-0.2054	-0.0148	-0.0148	0.19843	0.19842
0.1	0.00000	0.00000	-0.3021	-0.3021	-0.0619	-0.0619	0.27637	0.27637

Table 4. Comparisons of the transfer matrix method (TMM) and the complementary functions method (CFM) elastic fields in the exponential disk based on the Model-II (n=3)

$r(m)$	\bar{u}_r		$\bar{\sigma}_r$		$\bar{\sigma}_\theta$		$\bar{\sigma}_{eq}$	
	CFM	TMM	CFM	TMM	CFM	TMM	CFM	TMM
Free-Free								
0.01	0.05218	0.05218	0.00000	0.00000	0.52180	0.52180	0.52180	0.52180
0.019	0.06044	0.06043	0.19264	0.19262	0.37178	0.37173	0.32204	0.32200
0.028	0.08422	0.08421	0.24170	0.24167	0.36908	0.36904	0.32470	0.32466
0.037	0.11202	0.11200	0.25967	0.25964	0.37807	0.37803	0.33495	0.33491
0.046	0.14014	0.14012	0.26116	0.26112	0.38395	0.38390	0.33963	0.33958
0.055	0.16631	0.16629	0.24968	0.24963	0.38400	0.38395	0.33752	0.33747
0.064	0.18881	0.18879	0.22610	0.22606	0.37794	0.37789	0.32941	0.32936
0.073	0.20637	0.20635	0.19029	0.19025	0.36613	0.36608	0.31716	0.31712
0.082	0.21812	0.21810	0.14153	0.14150	0.34904	0.34900	0.30407	0.30404
0.091	0.22360	0.22358	0.07865	0.07862	0.32700	0.32697	0.29563	0.29561
0.1	0.22267	0.22267	0.00000	0.00000	0.30005	0.30005	0.30005	0.30005
Fixed-Free								
0.01	0.00000	0.00000	0.31979	0.31979	0.08830	0.08830	0.28605	0.28605
0.019	0.03686	0.03687	0.26684	0.26686	0.26788	0.26791	0.26737	0.26738
0.028	0.06945	0.06946	0.27240	0.27242	0.32434	0.32436	0.30174	0.30176
0.037	0.10132	0.10133	0.27583	0.27585	0.35302	0.35305	0.32145	0.32148
0.046	0.13169	0.13170	0.27077	0.27079	0.36751	0.36754	0.32996	0.32998
0.055	0.15923	0.15924	0.25577	0.25580	0.37194	0.37197	0.32959	0.32962
0.064	0.18259	0.18260	0.23005	0.23007	0.36831	0.36834	0.32225	0.32228
0.073	0.20070	0.20072	0.19280	0.19282	0.35791	0.35794	0.31027	0.31029
0.082	0.21281	0.21282	0.14300	0.14302	0.34165	0.34167	0.29718	0.29720
0.091	0.21850	0.21851	0.07930	0.07931	0.32007	0.32009	0.28871	0.28872
0.1	0.21770	0.21770	0.00000	0.00000	0.29335	0.29335	0.29335	0.29335
Fixed-Fixed								
0.01	0.00000	0.00000	0.14493	0.14493	0.04002	0.04002	0.12964	0.12964
0.019	0.01630	0.01630	0.11440	0.11440	0.11748	0.11749	0.11597	0.11598
0.028	0.02955	0.02955	0.10617	0.10618	0.13532	0.13533	0.12336	0.12337
0.037	0.04082	0.04082	0.09234	0.09235	0.13714	0.13716	0.12113	0.12114
0.046	0.04928	0.04929	0.06976	0.06977	0.12918	0.12919	0.11199	0.11200
0.055	0.05395	0.05395	0.03743	0.03744	0.11336	0.11337	0.10004	0.10005
0.064	0.05397	0.05397	-0.0054	-0.0054	0.09064	0.09065	0.09346	0.09347
0.073	0.04875	0.04875	-0.0597	-0.0597	0.06159	0.06160	0.10504	0.10504
0.082	0.03800	0.03800	-0.1266	-0.1266	0.02649	0.02650	0.14167	0.14167
0.091	0.02169	0.02169	-0.2075	-0.2075	-0.0147	-0.0147	0.20054	0.20054
0.1	0.00000	0.00000	-0.3043	-0.3043	-0.0623	-0.0623	0.27846	0.27846

Finally, Table 3 and 4 reveals that the results obtained by both methods overlap. Very minor differences between TMM and CFM solutions (the maximal relative error for the equivalent stress is about 10^{-4} for Model-I) may probably stem from the numerical integration technique used in TMM together with the FG orthotropic nature of the disk material and geometry. For example, when a uniform disk with power-law graded of a single orthotropic material is considered, two solution methods have been presented the same results to the seven digits after dot with the analytical solutions [61]. The maximum degree of precision numerical integration technique has been used in the present study in TMM. RK4 has been employed in CFM

solutions. When necessary, with the help of the properties of the transfer matrix method, it is also possible to increase the accuracy of the homogeneous and particular solutions without changing the accuracy of Runge-Kutta and numerical integration techniques.

6. Discussion

The complementary functions method (CFM) is one of the techniques in IVP solvers. It may be used directly or as an assistant tool as in the present study for solving some kinds of problems. The main feature of the problems to be directly handled by CFM is that there must not be any intermediate singular loads in the domain considered. For instance, the bending of a beam subjected to a singular force cannot be directly studied by CFM. To exemplify, concentric disks without the residual internal stresses may be studied by CFM by letting larger matrix dimensions. In these cases, both CPU time and the volume of the computer code also increase extremely.

The transfer matrix method (TMM) is a more general solution method than CFM. Many complex problems may be considered by TMM. For example, concentric disks may be studied by TMM without increasing the size of matrices and also considering the residual internal stresses at the intermediate contact surfaces of the disks. Due to these reasons, and to build a foundation for such kinds of advanced problems [77-81], the transfer matrix method solution technique in which the transfer matrix has been obtained with the help of CFM is preferred in this study.

In the method of CFM, the general solution of BVP in Eq. (4) reads [49]

$$u_r(r) = u_r^{(0)}(r) + b_1 u_r^{(1)}(r) + b_2 u_r^{(2)}(r) \quad (18)$$

Where $u_r^{(1)}(r)$ and $u_r^{(2)}(r)$ characterize the homogeneous solutions of Eq. (4) under prescribed Kronecker delta initial conditions ($u_r(a)=1$ and $du_r(r)/dr|_{r=a}=0$ for the determination of $u_r^{(1)}(r)$; and $u_r(a)=0$ and $du_r(r)/dr|_{r=a}=1$ for the determination of $u_r^{(2)}(r)$) while $u_r^{(0)}(r)$ is the nonhomogeneous solutions of Eq. (4) under zero initial conditions ($u_r(a)=0$ and $du_r(r)/dr|_{r=a}=0$); b_1 , and b_2 are the other unknowns which are determined by plugging the physical boundary conditions in the solution (18). CFM solutions for both the radial displacement and the radial stress may be written in a compact form as

$$\begin{Bmatrix} u_r(r) \\ \sigma_r(r) \end{Bmatrix} = \begin{bmatrix} u_r^{(1)}(r) & u_r^{(2)}(r) \\ \sigma_r^{(1)}(r) & \sigma_r^{(2)}(r) \end{bmatrix} \begin{Bmatrix} b_1 \\ b_2 \end{Bmatrix} + \begin{Bmatrix} u_r^{(0)}(r) \\ \sigma_r^{(0)}(r) \end{Bmatrix} \quad (19)$$

Yıldırım [49] also showed that the CFM solution inherently covers the fundamental matrix or the transfer matrix by an alias, as follows

$$\mathbf{F}(a,r) = \begin{bmatrix} u_r^{(1)}(r) & u_r^{(2)}(r) \\ \sigma_r^{(1)}(r) & \sigma_r^{(2)}(r) \end{bmatrix} \begin{bmatrix} u_r^{(1)}(a) & u_r^{(2)}(a) \\ \sigma_r^{(1)}(a) & \sigma_r^{(2)}(a) \end{bmatrix}^{-1} \quad (20)$$

As stated above, the accuracy of the numerical results strictly depends on the accuracy of the numerical transfer matrix. Both the material orthotropy [61] and the thickness gradient [49]

significantly influence the accuracy of the transfer matrix. After the determination of the elements of the transfer matrix with a desired accuracy within the acceptable engineering errors, the solution is obtained by employing Eq. (8) in the transfer matrix method (see Appendix).

In practice, a small part of the radial coordinate may be graded. The whole disk may compose of several disks with different profiles. The residual internal stresses due to the shrinking process including hub and blade pressures should be included in the analysis. As stated above, the transfer matrix method is to be a very useful choice for the solution of such types of problems. The author aims to step-by-step study more advanced problems based on the well-founded analytical and numerical results.

7. Conclusions

Minimizing weight and maximizing strength in gas turbine discs in the aerospace industry, such as turbojet engines, are the main practical applications of functionally graded and rotating discs of varying thickness. Since there is no single FG-material type or thickness variation function that can be a recipe for all kinds of problems, different thickness functions (linear, exponential, hyperbolic, parabolic, etc.) and basic properties of FG-material components (isotropic, orthotropic, etc.) are currently studied in the existing literature. Contrary to producing inhomogeneous material from two isotropic materials, unfortunately, the number of studies based on inhomogeneous material from two orthotropic materials is not yet sufficient as the problem becomes more complex. One of the main aims of this study is to fill this gap to some extent with numerical solutions having acceptable precision.

The problem chosen involves an elastic analysis of exponentially varying thickness rotating disks under three boundary conditions. Two orthotropic materials are graded based on a simple Voigt mixture rule with powers of volume fraction of constituents as the disk inhomogeneous and orthotropic material. Two models are used in the volume fraction of constituents. Results are tabulated and illustrated in graphical forms. There are no such significant differences in CPU-time and accuracy in the solutions by the two methods for the proposed example in which the disk consists of a single body having continuously varying material and thickness properties.

Previous studies showed that decreasing thickness profiles from the inner surface towards the outer propose more suitable stress distributions than the uniform ones under centrifugal forces. Another scope of the present study is to have a comparison of two Voigt grading models for the same disk thickness profile. For the chosen material and disk profile whose thickness smoothly decreases from the inner surface towards the outer, in general, such remarkable differences are not observed between the results of the two material grading models for $n > 1$. They may be much more noticeable when different profiles and different orthotropic materials having different orthotropy degrees are used. Besides, if Model-I is used, the choice of inhomogeneity indexes, which are equal to or greater than 0.5, may be recommended.

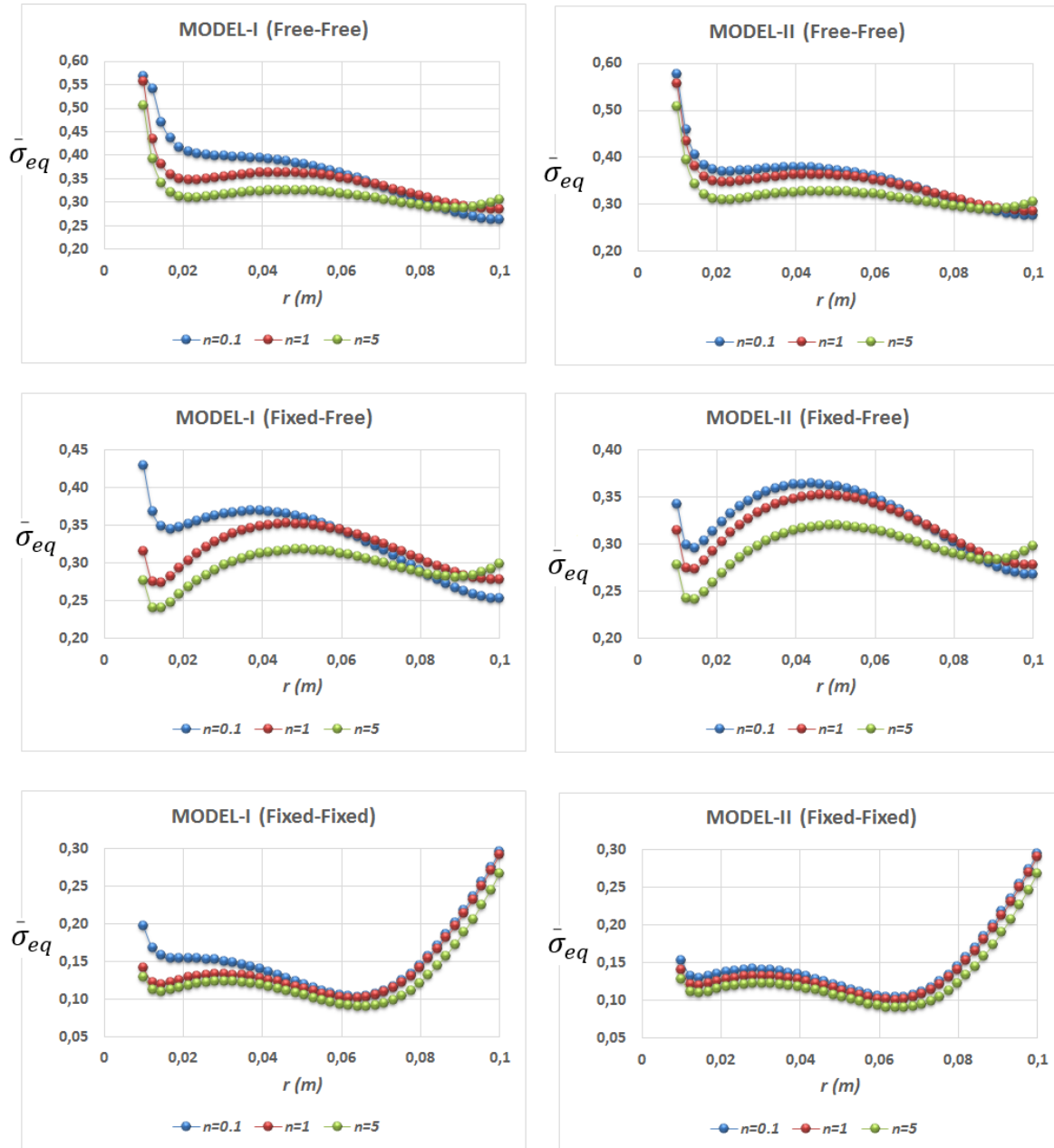
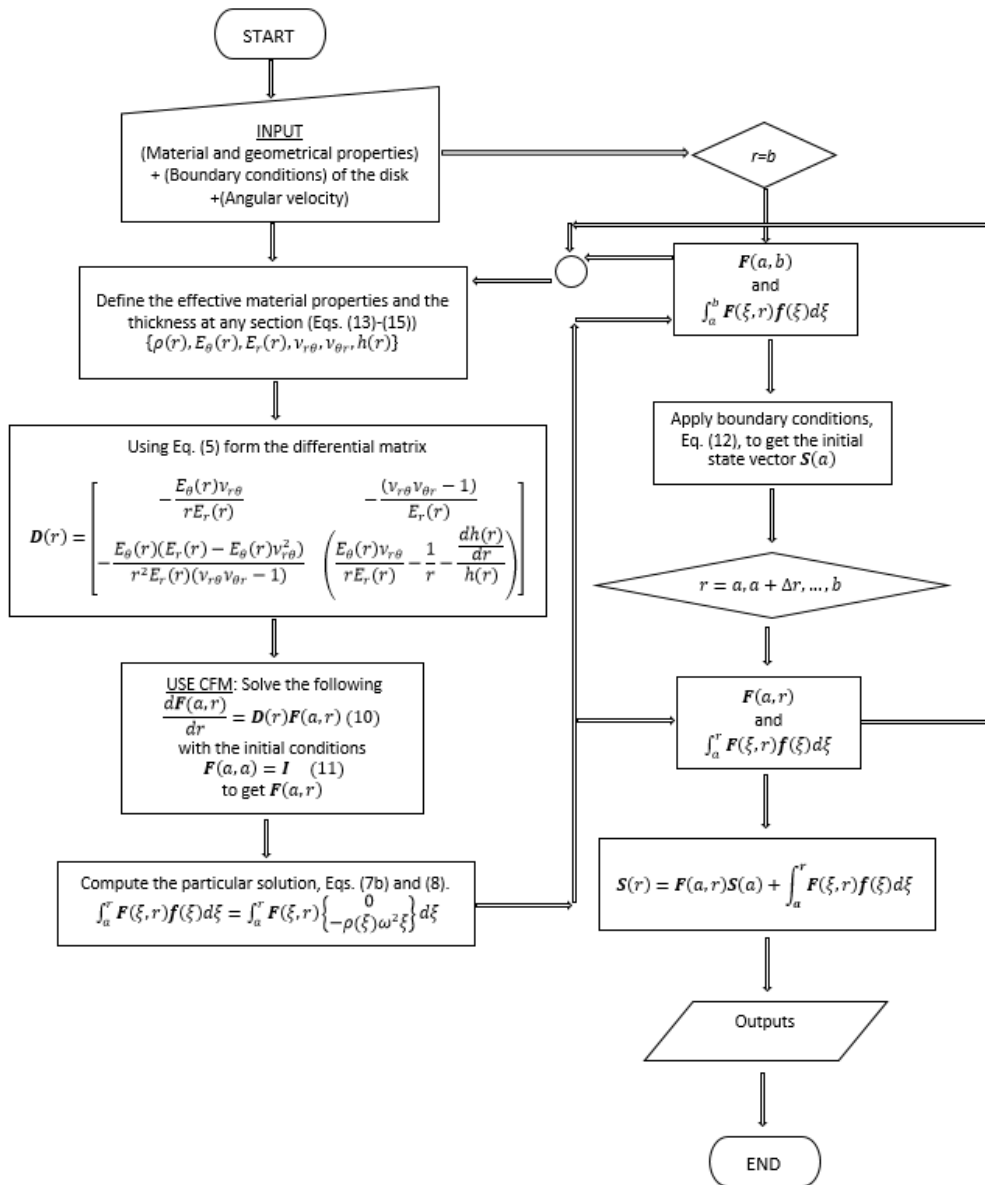


Fig. 7. Dimensionless equivalent stresses under three boundary conditions based on the two models.

Appendix: Flowchart of TMM procedure



Declaration of Conflicting Interests

The author(s) declared no potential conflicts of interest concerning the research, authorship, and/or publication of this article.

Acknowledgement

The author thanks the referees for their very useful suggestions, rigorous reviews, and precious time spent.

Notations

a, b	Inner and outer radii of the disk
C_{ij} ($i = 1,2$ and $j = 1,2$)	Transformed on-axis in-plane stiffness terms
D	Differential matrix
E_r, E_θ	Anisotropic Young's moduli
f	Nonhomogeneous vector
F	Transfer matrix
h	thickness
I	Unit matrix
k, m	Constants for the disk profile
n	Inhomogeneity index
r, θ	Radial and circumferential coordinates
S	State vector
u_r	Radial displacement
V_A, V_B	Volume fractions of Materials A and B
ω	Angular velocity
$\varepsilon_r, \varepsilon_\theta$	Radial and circumferential strains
$\nu_{r\theta}, \nu_{\theta r}$	Anisotropic Poisson's ratios
ρ	Material density
σ_{eq}	Von-Mises equivalent stress
σ_r, σ_θ	Radial and circumferential stresses

References

- [1]Tang S. Elastic stresses in rotating anisotropic discs. *Int J Mech Sci* (IJMS), 11, 509–517, 1969.
- [2]Murthy D, Sherbourne A. Elastic stresses in anisotropic discs of variable thickness. *Int J Mech Sci*, 12, 627-640, 1970.
- [3]Reddy TY, Srinath H. Elastic stresses in a rotating anisotropic annular disc of variable thickness and variable density. *Int J Mech Sci*, 16(2), 85-89, 1974.
- [4]Chang CI. A closed-form solution for an orthotropic rotating disc. *J Appl Mech*, 41(4), 1122–1123, 1974.
- [5]Chang CI. The anisotropic rotating discs. *Int J Mech Sci* 1975; 17(6): 397-402.
- [6]Bert CW. Centrifugal stresses in arbitrarily laminated, rectangular-anisotropic circular discs. *J Strain Anal Eng Des*, 10, 84-92, 1975.
- [7]Gurushankar GV. Thermal stresses in a rotating nonhomogeneous, anisotropic disc of varying thickness and density. *J Strain Anal Eng Des*, 10, 137-142, 1975.
- [8]Christensen RM, Wu EM. Optimal design of anisotropic (fiber-reinforced) flywheels. *J Compos Mater*, 11, 395-404, 1977.

- [9]Belingardi G, Genta G, Gola M. A study of the stress distribution in rotating, orthotropic discs. *Composites*, 10(2), 77-80, 1979.
- [10]Genta G, Gola M. The stress distribution in orthotropic rotating discs. *J Appl Mech*, 48, 559-562, 1981.
- [11]Jain R, Ramachandra K, Simha KRY. Rotating anisotropic disk of uniform strength. *Int J Mech Sci*, 41, 639–648, 1999.
- [12]Tutuncu N. Effect of anisotropy on stresses in rotating discs. *Int J Mech Sci*, 37, 873–881, 2000.
- [13]Zhou F, Ogawa A. Elastic solutions for a solid rotating disc with cubic anisotropy. *J Appl Mech*, 69, 81-83, 2002.
- [14]Callioglu H. Stress analysis of an orthotropic rotating disc under thermal loading. *J Reinf Plast Compos*, 23(17), 1857–1869, 2004.
- [15]Callioglu H, Topcu M, Altan G. Stress analysis of curvilinearly orthotropic rotating discs under mechanical and thermal loading. *J Reinf Plast Compos*, 24, 831-838, 2005.
- [16]Sayer M, Topcu M, Bektas NB, Tarakçılar AR. Thermoelastic stress analysis in a thermoplastic composite disc. *Sci Eng Compos Mater*, 12(4), 251–260, 2005.
- [17]Tahani M, Nosier A, Zebarjad SM. Deformation and stress analysis of circumferentially fiber-reinforced composite disks. *Int J Solids Struct*, 42(9-10), 2741–2754, 2005.
- [18]Zenkour AM, Allam NMN. On the rotating fiber-reinforced viskoelastic composite solid and annular disks of variable thickness. *Int J Comput Methods Eng Sci Mech*, 7, 21-31, 2006.
- [19]Callioglu H, Topcu M, Tarakçılar AR. Elastic-plastic stress analysis of an orthotropic rotating disc. *Int J Mech Sci*, 48, 985-990, 2006.
- [20]Callioglu H. Thermal stress analysis of curvilinearly orthotropic rotating discs. *J Thermoplast Compos Mater*, 20, 357-369, 2007.
- [21]Alexandrova N, Vila Real PMM. Deformation and stress analysis of an anisotropic rotating annular disk. *Int J Comput Methods Eng Sci Mech*, 9(1), 43–50, 2008.
- [22]Sen F, Koruvatan T, Aldas K, Thermal residual stresses in thermoplastic composite disc with holes using 3D-FEM. *Adv Compos Lett*, 23(4), 79-87, 2014.
- [23]Eraslan AN, Kaya Y, Varlı E. Analytical solutions to orthotropic variable thickness disk problems. *Pamukkale University Journal of Engineering Sciences*, 22(1), 24–30, 2016.
- [24]Yıldırım V. The complementary functions method (CFM) solution to the elastic analysis of polar orthotropic rotating discs. *Journal of Applied and Computational Mechanics (JACM)*, 4(3), 216-230, 2018. DOI: [10.22055/JACM.2017.23188.1150](https://doi.org/10.22055/JACM.2017.23188.1150)
- [25]Horgan C, Chan A. The pressurized hollow cylinder or disk problem for functionally graded isotropic linearly elastic materials. *J Elasticity*, 55, 43-59, 1999.

- [26]Horgan C, Chan A. The stress response of functionally graded isotropic linearly elastic rotating disks. *J Elasticity*, 55, 219-230, 1999.
- [27]Zenkour AM. Analytical solutions for rotating exponentially-graded annular disks with various boundary conditions. *Int J Struct Stab Dy*, 5, 557-577, 2005.
- [28]Eraslan AN, Akiş T. On the plane strain and plane stress solutions of functionally graded rotating solid shaft and solid disk problems. *Acta Mechanica*, 181(1–2), 43–63, 2006.
- [29]Zenkour AM. Elastic deformation of the rotating functionally graded annular disk with rigid casing. *J Mater Sci*, 42, 9717-9724, 2007.
- [30]You LH, You XY, Zhang JJ, Li J. On rotating circular disks with varying material properties. *Zeitschrift für angewandte Mathematik und Physik ZAMP*, 58, 1068–1084, 2007.
- [31]Bayat M, Saleem M, Sahari B, Hamouda A, Mahdi E. Analysis of functionally graded rotating disks with variable thickness. *Mech Res Commun*, 35, 283-309, 2008.
- [32]Vivio F, Vullo V. Elastic stress analysis of rotating converging conical disks subjected to thermal load and having variable density along the radius. *Int J Solids Struct*, 44, 7767–7784, 2007.
- [33]Vullo V, Vivio F. Elastic stress analysis of non-linear variable thickness rotating disks subjected to thermal load and having variable density along the radius. *Int J Solids Struct*, 45, 5337–5355, 2008.
- [34]Hojjati MH, Jafari. S Semi exact solution of elastic non uniform thickness and density rotating disks by Homotopy Perturbation and Adomian's decomposition methods Part I: Elastic solution. *Int J Pres Ves Pip*, 85, 871-878, 2008.
- [35]Hojjati MH, Hassani A. Theoretical and numerical analyses of rotating discs of nonuniform thickness and density. *Int J Pres Ves Pip*, 85, 694-700, 2008.
- [36]Nie GJ, Batra RC. Stress analysis and material tailoring in isotropic linear thermoelastic incompressible functionally graded rotating disks of variable thickness. *Compos Struct*, 92, 720-729, 2010.
- [37]Çallıoğlu H, Bektaş NB, Sayer M. Stress analysis of functionally graded rotating discs: Analytical and numerical solutions. *Acta Mech Sinica*, 27, 950-955, 2011.
- [38]Hassani A, Hojjati MH, Farrahi G, Alashti RA. Semi-exact elastic solutions for thermomechanical analysis of functionally graded rotating disks. *Compos Struct*, 93, 3239-3251, 2011.
- [39]Zenkour AM, Mashat DS. Stress function of a rotating variable-thickness annular disk using exact and numerical methods. *Engineering*, 3, 422-430, 2011.
- [40]Argeso H. Analytical solutions to variable thickness and variable material property rotating disks for a new three-parameter variation function. *Mech Based Des Struc*, 40, 133-152, 2012.

- [41]Nejad MZ, Abedi M, Lotfian MH, Ghannad M. Elastic analysis of exponential FGM disks subjected to internal and external pressure. *Central European Journal of Engineering*, 3, 459-465, 2013.
- [42]Nejad MZ, Rastgoo A, Hadi A. Exact elasto-plastic analysis of rotating disks made of functionally graded materials. *Int J Eng Sci*, 85, 47-57, 2014.
- [43]Eraslan AN, Arslan E. Analytical and numerical solutions to a rotating FGM disk. *Journal of Multidisciplinary Engineering Science and Technology (JMEST)*, 2(10), 2843-2850, 2015.
- [44]Yıldırım V. Analytic solutions to power-law graded hyperbolic rotating discs subjected to different boundary conditions. *International Journal of Engineering & Applied Sciences (IJEAS)*, 8(1), 38-52, 2016.
- [45]Yıldırım V, Kacar İ. Introducing a computer package program for elastic analysis of functionally graded rotating thick-walled annular structures. *Digital Proceeding of ICOCEE – Cappadocia 2017, S. Sahinkaya and E. Kalıpcı (Editors), Nevsehir, TURKEY, May 8-10, 1733-1742, 2017.*
- [46]Yıldırım V. Effects of inhomogeneity and thickness parameters on the elastic response of a pressurized hyperbolic annulus/disc made of functionally graded material. *International Journal of Engineering & Applied Sciences (IJEAS)*, 9(3), 36-50, 2017. DOI: 10.24107/ijeas.329433
- [47]Gang M. Stress analysis of variable thickness rotating FG disc. *International Journal of Pure and Applied Physics*, 13(1), 158-161, 2017.
- [48]Yıldırım V. A parametric study on the centrifugal force-induced stress and displacements in power-law graded hyperbolic discs. *Lati Am J Solids Stru (LAJSS)*, 15(4), 1-16, 2018.
- [49]Yıldırım V. Numerical elasticity solution for continuously tapered and arbitrarily functionally graded (FG) rotating disks via the transfer matrix approach. *International Journal of Mathematics and Computational Science*, 4(2), 48-73, 2018.
- [50]Khorsand M, Tang Y. Design functionally graded rotating disks under thermoelastic loads: Weight optimization. *Int J Pres Ves Pip*, 161, 33–40, 2018.
- [51]Durodola J, Attia O. Deformation and stresses in functionally graded rotating discs. *Compos Sci Technol*, 60, 987-995, 2000.
- [52]Chen J, Ding H, Chen W. Three-dimensional analytical solution for a rotating disc of functionally graded materials with transverse isotropy. *Archive of Applied Mechanics*, 77, 241-251, 2007.
- [53]Nie GJ, Zhong Z, Batra RC. Material tailoring for orthotropic rotating disks. *Compos Sci Technol*, 71, 406-414, 2011.
- [54]Kansal G, Parvez M. Thermal stress analysis of orthotropic graded rotating discs. *International Journal of Modern Engineering Research (IJMER)*, 2(5), 3881-3885, 2012.

- [55]Lubarda VA. On pressurized curvilinearly orthotropic circular disc, cylinder and sphere made of radially nonuniform material. *J Elasticity*, 109, 103-133, 2012.
- [56]Peng XL, Li XF. Elastic analysis of rotating functionally graded polar orthotropic discs. *Int J Mech Sci (IJMS)*, 60, 84-91, 2012.
- [57]Kacar I, Yildirim V. Effect of the anisotropy ratios on the exact elastic behavior of functionally power-graded polar orthotropic rotating uniform discs under various boundary conditions. *Digital Proceeding of ICOCEE – Cappadocia 2017, Nevsehir, Turkey*, 1743-1752, 2017.
- [58]Essa S, Argeso H. Elastic analysis of variable profile and polar orthotropic FGM rotating disks for a variation function with three parameters. *Acta Mechanica*, 228, 3877–3899,2017.
- [59]Zheng Y, Bahaloo H, Mousanezhad D, Vaziri A, Nayeb-Hashemi H. Displacement and stress fields in a functionally graded fiber-reinforced rotating disk with nonuniform thickness and variable angular velocity. *J Eng Mater-T ASME*, 39, 031010-1-9, 2017.
- [60]Yildirim V. Unified exact solutions to the hyperbolically tapered pressurized/rotating disks made of nonhomogeneous isotropic/orthotropic materials. *International Journal of Advanced Materials Research*, 4(1), 1-23, 2018.
- [61]Yildirim V. Numerical/analytical solutions to the elastic response of arbitrarily functionally graded polar orthotropic rotating discs. *J Braz Soc Mech Sci & Eng*, 40, 1-21, 2018.
- [62]İnan M. *The Method of Initial Values and the Carry-Over Matrix in Elastomechanics*. ODTÜ M., Publication, Ankara, No: 20, 1968.
- [63]Haktanır V, Kiral E. Statical analysis of elastically and continuously supported helicoidal structures by the transfer and stiffness matrix methods. *Computers and Structures*,49(4), 663-677, 1993.
- [64]Chen YZ, Lin XY. An alternative numerical solution of thick-walled cylinders and spheres made of functionally graded materials. *Comp Mater Sci*, 48, 640–647, 2010.
- [65]Arici M, Granata MF. Generalized curved beam on elastic foundation solved by Transfer Matrix Method. *Structural Engineering & Mechanics*, 40(2), 279-295, 2011.
- [66]Garus S, Sochacki W. One dimensional phononic FDTD algorithm and transfer matrix method implementation for severin aperiodic multilayer. *Journal of Applied Mathematics and Computational Mechanics*, 16(4), 17-27, 2017.
- [67]Wimmer H, Nachbagauer K. Exact transfer- and stiffness matrix for the composite beam-column with refined zigzag kinematics. *Compos Struct*,189, 700-706, 2018.
- [68]Zhong H, Liu Z, Qin H, Liu Y. Static analysis of thin-walled space frame structures with arbitrary closed cross-sections using transfer matrix method. *Thin Wall Struct*, 123, 255-269, 2018.
- [69]Yildirim V. Several stress resultant and deflection formulas for Euler-Bernoulli beams under concentrated and generalized power/sinusoidal distributed loads. *International*

Journal of Engineering & Applied Sciences (IJEAS), 10(2), 35-632018. DOI: 10.24107/ijeas.430666

- [70] Aktas Z. *Numerical Solutions of Two-Point Boundary Value Problems*. Ankara, Turkey, METU, Dept of Computer Eng, 1972.
- [71] Roberts S, Shipman J. Fundamental matrix and two-point boundary-value problems. *J Optimiz Theory App*, 28(1), 77-88, 1979.
- [72] Haktanir V, Kiral E. Direct application of complementary functions method to axisymmetrical shells and cylindrical vaults (barrels). *Journal of Isparta Eng Faculty of Akdeniz Un.*, 6, 220-239, 1991.
- [73] Haktanir V. The complementary functions method for the element stiffness matrix of arbitrary spatial bars of helicoidal axes. *Int J Numer Meth Eng*, 38(6), 1031–1056, 1995. Doi:10.1002/nme.1620380611
- [74] Yildirim V. Free vibration analysis of non-cylindrical coil springs by combined use of the transfer matrix and the complementary functions methods. *Commun Numer Meth Eng*, 13(6), 487–494, 1997.
- [75] Yildirim V. A parametric study on the natural frequencies of unidirectional composite conical springs. *Commun Numer Meth Eng*, 20(3), 207–227, 2004.
- [76] Eraslan AN, Orcan Y. Elastic–plastic deformation of a rotating solid disk of exponentially varying thickness. *Mech Mater*, 34, 423-432, 2002.
- [77] Yildirim, V. The best grading pattern selection for the axisymmetric elastic response of pressurized inhomogeneous annular structures (sphere/ cylinder/annulus) including rotation. *Journal of the Brazilian Society of Mechanical Sciences and Engineering*. 42:109, 2020. <https://doi.org/10.1007/s40430-020-2193-x>
- [78] Avcar M., Hadji L., Civalek Ö. Natural frequency analysis of sigmoid functionally graded sandwich beams in the framework of high order shear deformation theory. *Composite Structures*, 276, 114564, 2021. <https://doi.org/10.1016/j.compstruct.2021.114564>.
- [79] Hadji L., Avcar M., Zouatnia N. Natural frequency analysis of imperfect FG sandwich plates resting on Winkler-Pasternak foundation. *Materials Today: Proceedings*, 53(1), 153-160, 2022. <https://doi.org/10.1016/j.matpr.2021.12.485>.
- [80] Civalek, Ö., Avcar, M. Free vibration and buckling analyses of CNT reinforced laminated non-rectangular plates by discrete singular convolution method. *Engineering with Computers*. 2020. <https://doi.org/10.1007/s00366-020-01168-8>
- [81] Arslan E., Mack W., Apatay T. Thermo-mechanically loaded steel/aluminum functionally graded spherical containers and pressure vessels. *International Journal of Pressure Vessels and Piping*. 191, 104334, 2021. <https://doi.org/10.1016/j.ijpvp.2021.104334>